Available online at
https://jmeche.uitm.edu.my/

e-ISSN: 2550-164X

Journal of Mechanical Engineering 23(2) 2026, 171 – 186.

Journal of Mechanical Engineering

Real-Time Stress and Strain Measurement in Bolted Flanges Using FBG Sensors For Enhanced Sustainability and Leak Prevention

Muhammad Abdullah[1], Mohd Hafizi Zohari[1,2*], Ihsan Naiman Ibrahim[1]

[1]*Advanced Structural Integrity and Vibration Research (ASIVR), Faculty of Mechanical & Automotive Engineering Technology, Universiti Malaysia Pahang Al-Sultan Abdullah (UMPSA), Malaysia*
[2]*Centre for Advanced Industrial Technology, Universiti Malaysia Pahang Al-Sultan Abdullah, 26600 Pekan, Pahang*

ARTICLE INFO

Article history:
Received 21 October 2025
Revised 15 January 2026
Accepted 22 April 2026
Published 15 May 2026

Keywords:
Fiber Bragg Grating (FBG) sensors
FBG-embedded bolts
Bolted flange joints
Real-time preload monitoring
Structural health monitoring (SHM)

DOI:
10.24191/jmeche.v23i2.11765

ABSTRACT

Bolted flange joints are critical components in pressure retaining and structural systems, where maintaining proper preload is essential for sealing integrity and mechanical reliability. Conventional torque-based tightening methods often result in inconsistent preload due to frictional variations and the absence of real-time monitoring. This inconsistency arises because friction can vary from bolt to bolt, leading to uneven preload even when the same torque is applied. Real-time monitoring enables precise preload verification and adjustment, ensuring uniformity and reducing the risk of failure. This study develops and validates Fibre Bragg Grating (*FBG*) embedded stud bolts for real-time preload measurement. Four M18 carbon steel grade 8.8 bolts were tested under incremental torque from 10 to 80 *Nm* at room temperature, with wavelength shifts converted using an optical interrogation system. The results show a near-linear torque–wavelength relationship, with measured sensitivities of 0.0100, 0.0123, 0.0120, and 0.0080 *nm/N·m* for Bolts *B1*, *B2*, *B3*, and *B4*, respectively, and R^2 values of 0.946, 0.974, 0.939, and 0.974, confirming consistent sensitivity ranking and stable sensor performance. Wavelength shifts ranged from approximately 0.08 to 1.07 *nm* at 80 *Nm*. These findings demonstrate that *FBG*-embedded bolts provide a reliable, non-intrusive solution for continuous preload monitoring, improving load control accuracy and enabling predictive maintenance in high-reliability industries such as oil and gas or aerospace.

INTRODUCTION

Bolted flange joints (*BFJs*) are critical components in various industries such as oil and gas, aerospace, defence environments, and chemical processing (Silva & Sakamoto, 2026). They reliably connect pipes and pressure vessels in systems handling pressurized fluids or gases. Understanding the function and

[2*] Corresponding author. *E-mail address*: hafizi@umpsa.edu.my
https://doi.org/10.24191/jmeche.v23i2.11765

integrity of these joints is vital for maintaining the safety and efficiency of industrial system. The reliability of *BFJs* is essential for the stable operation of pressure retaining and structural system. Failures in these joints can lead to severe environmental hazards, significant economic losses, production disruptions, and higher maintenance costs (Nelson et al., 2023). Fig. 1 presents a schematic diagram of the *BFJ*. The nut-bolt assembly applies a preload, which clamps the two flanges against the gasket, establishing initial sealing stress. The gasket generates a reactive force that resists separation, while external loads, such as pressure, thermal, and mechanical actions, act on the joint and are shared by the bolts and gasket. During service, loss or redistribution of and uneven sharing of among the bolts reduce effective gasket stress, increasing the likelihood of leakage.

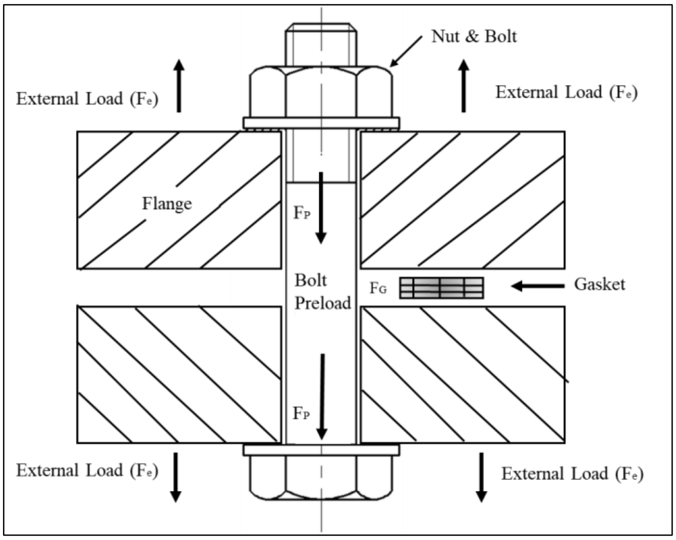

Fig. 1. Schematic illustration of bolted flange joint (Nelson et al., 2023).

The performance of *BFJs* is affected by factors like bolt relaxation and uneven load distribution, which undermine sealing integrity and elevate the risk of leakage (Zheng et al., 2016; Bouzid & Nechache, 2004; Nechache & Bouzid, 2008; Nechache & Bouzid, 2007). Furthermore, fluctuating temperatures further increase these challenges, reducing joint performance. Therefore, to achieve consistent preload across bolts remains a significant challenge due to uneven load distribution, which can cause gasket deformations and sealing failure (Zhu et al., 2018). As a result, bolted flange joints become more vulnerable to leakage and structural degradation during prolonged service. Gasket failures can pose safety risks, environmental contamination, and resource losses, emphasizing the need for improved joint integrity under varying operating conditions (Aycock et al., 2019; Khan et al., 2017).

Conventional torque-based tightening, ultrasonic, and piezoelectric methods often fail to ensure uniform preload across multiple bolts, resulting in uneven load distribution and increased leakage susceptibility. In high-pressure systems such as pipelines and pressure vessels, traditional bolted joints are prone to degradation due to factors like uneven load distribution, and mechanical fatigue (Abdullah et al., 2025; Radzi & Zohari, 2023). These issues contribute to premature joint failure, leading to unplanned maintenance, increased downtime, frequent replacements, and heightened vulnerability to leakage (La Salandra et al., 2016). This underscores the need for continuous monitoring solutions that track bolt conditions during service rather than relying on discrete inspections.

To address this gap, *FBG* sensors offer real-time, continuous monitoring for precise strain measurement and load distribution control. By embedding *FBG* sensors directly into the bolts, real-time stress and strain

https://doi.org/10.24191/jmeche.v23i2.11765

monitoring becomes possible, enabling early detection of issues such as bolt loosening, gasket deformation, or material fatigue (Moravcik et al., 2026; Zhu et al., 2018). This real-time monitoring reduces the need for frequent maintenance and unnecessary inspections, contributing to the sustainability of industrial operations extending system lifespans (Bouzid & Nechache, 2010; Nechache et al., 2004). This is especially crucial in industries where the safety of pressurized systems is paramount, such as oil and gas, nuclear, and chemical sectors. *FBG*-based monitoring directly addresses the limitations of current monitoring methods, particularly in ensuring continuous monitoring of joint conditions. Beyond the technical benefits, a proactive monitoring approach minimizes operational downtime and supports the efficient and sustainable operation of industrial systems. By reducing maintenance related waste and resource consumption and preventing leaks, the system helps maintain safety and environmental standards while aligning with sustainability goals. Real-time monitoring with *FBG* sensors improves resource efficiency by enabling precise predictive maintenance, optimizing asset management, and minimizing waste. Reducing the frequency of manual inspections allows companies to focus resources on essential repairs, ensuring efficient allocation (Park & Park, 2014; Todd et al., 2006). *FBG* sensors also enable precise load distribution, reducing the risks of over-tightening or under-tightening, prolonging system life, and minimizing waste (Cloostermans et al., 2025).

This present study tests *FBG* sensors for real-time strain and load monitoring in bolted flange joints (*BFJs*). Embedding sensors improves detection of bolt loosening, gasket deformation, and material fatigue, which threaten joint integrity. The primary contribution of this study is to demonstrate higher sensitivity than previously reported bolt-integrated systems while maintaining the mechanical integrity of the bolt. The improved sensitivity results from enhanced strain transfer between the bolt substrate and the embedded *FBG*, leading to increased wavelength response per unit load. The groove-based embedding strategy reduces stress concentration and avoids significant alteration of the stress distribution within the M18 bolt, thereby preserving its load-carrying capacity. This approach enhances efficiency and supports sustainability through precise load distribution and predictive maintenance.

Theoretical modelling of *FBG* strain sensing

FBG sensors have become a fundamental technology in optical sensing. *FBG* plays a critical role in structural health monitoring by enabling real-time measurement of stress and strain in bolted joints, owing to their high sensitivity, resistance to electromagnetic interference, and multiplexing capability. An *FBG* is formed by creating a periodic modulation of the refractive index within the core of a single-mode optical fibre, typically using ultraviolet laser interference or a phase mask process (Bhatti et al., 2024). This modulation produces a microscopic grating, usually a few mm long, with a core diameter of about 8μm and an overall fibre diameter ranging from 125 to 250 μm, depending on the coating. The grating functions as a wavelength-selective reflector; when broadband light passes through the fibre, the *FBG* reflects a specific spectral band known as the Bragg wavelength, allowing other wavelengths to pass with minimal loss. This reflection enables precise detection of environmental changes based on the Bragg condition, which defines the wavelength at which constructive interference occurs within the periodic refractive index structure (Hadeed et al., 2025). The Bragg wavelength, denoted as, is expressed by the equation:

$$\lambda_B = 2\eta_{eff}\Lambda \tag{1}$$

where η_{eff} is the effective refractive index of the fiber core mode (typically around 1.45 for silica fibers), and Λ is the grating period. This equation highlights that any external factor altering either η_{eff} or Λ will induce a shift in forming the basis for sensing applications. Strain sensitivity arises from the mechanical deformation of the fiber, which modifies both the grating period through physical elongation/compression and the refractive index via the photoelastic effect. The relative shift in Bragg wavelength due to axial strain, and temperature change is given by:

https://doi.org/10.24191/jmeche.v23i2.11765

$$\frac{\Delta\lambda_B}{\lambda_B} = (1 - p_e)\varepsilon + (\alpha + \xi)\Delta T \quad (2)$$

where p_e is the effective photoelastic coefficient, typically approximately 0.22 for silica fibers incorporating strain-optic coefficients p_{11} and p_{12} around 0.12 and 0.27, respectively, and Poisson's ratio $v \approx 0.17$, as given by:

$$p_e = \frac{n_{eff}^2}{2}\left[p_{12} - \mathrm{v}\,(p_{11} + p_{12})\right] \quad (3)$$

For a standard *FBG* operating at 1550 nm, this yields a strain sensitivity of approximately 1.2 $pm/\mu\varepsilon$, meaning a 1 micro strain change induces a 1.2 $pm/\mu\varepsilon$. Enhancements to this sensitivity can be achieved through specialized packaging, such as *UV*-curable resin coatings, increasing it to about 1.5 $pm/\mu\varepsilon$ or structural amplifications like lever mechanisms for higher-resolution applications. Temperature effects must also be considered, as they are coupled with strain measurements primarily through the thermo-optic effect on η_{eff} and secondary thermal expansion of Λ. The relative wavelength shifts due to temperature change are (ΔT), where α is the thermal expansion coefficient of the fiber ($\approx 0.55 \times 10^{-6}/°C$), and ξ is the thermo-optic coefficient around ($5 \times 10^{-6}/°C$ - $8.6 \times 10^{-6}/°C$). This results in a typical temperature sensitivity of 10–13 *pm/°C* at 1550 *nm*. To mitigate cross-sensitivity in practical deployments, such as bolt monitoring, compensation techniques like reference gratings or dual-parameter sensors are employed to decouple strain from temperature effects. Temperature effects were neglected in this study since all experiments were conducted under controlled ambient temperature conditions.

EXPERIMENTAL SETUP

The experimental setup used an *ANSI B16.5* 3-inch flange rated for pressure class 150. *M18* carbon steel grade 8.8 bolts were used for fastening, and each bolt was machined with a shallow groove on the shank to place an *FBG* sensor for real-time strain monitoring, as shown in Fig. 2 (Yang et al., 2023). The material had a Young's modulus of 210 *GPa*, a Poisson's ratio of 0.3, an ultimate tensile strength of 840 *MPa*, and a yield strength of 600 *MPa*, ensuring stable performance under loading. Torque was applied to each bolt with a torque wrench, beginning at 10 *Nm* and increasing up to 80 *Nm* in *10 Nm* increments to record the strain change at each stage. To ensure data accuracy, measurements were repeated for all four bolts, each equipped with an *FBG* sensor of distinct wavelengths: 1548 *nm*, 1550 *nm*, 1552 *nm*, and 1554 *nm*.

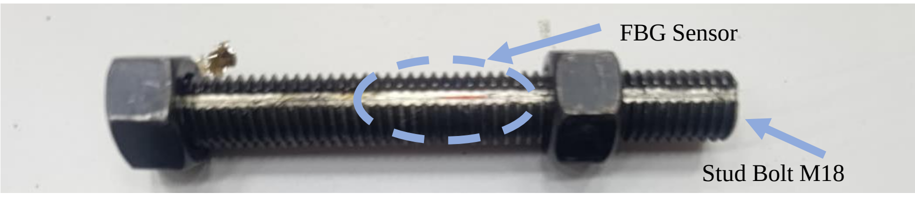

Fig. 2. *FBG* embedded on M18 stud bolts.

Fig. 3 and Fig. 4 illustrate the *FBG* interrogation system and its components, which are critical for accurately recording wavelength shifts from the FBG sensor, corresponding to variations in strain. The system operates by utilizing a Super Luminescent Diode (*SLD*) broadband light source, which provides stable and consistent optical output necessary for the illumination of the *FBG* sensor. The light from the *SLD* source interacts with the sensor, and the reflected light carries information about strain changes. The *FBG* interrogator then analyzes these wavelength shifts and converts them into strain measurements,

https://doi.org/10.24191/jmeche.v23i2.11765

allowing real-time monitoring of the strain in bolted joints. An optical circulator is integrated into the system to efficiently direct the light between the various ports, ensuring that the light reaches the *FBG* sensor with minimal loss and preserving the signal integrity. These components collectively enable precise real-time strain measurement, ensuring the bolted joints structural integrity under applied torque throughout the experimental procedure.

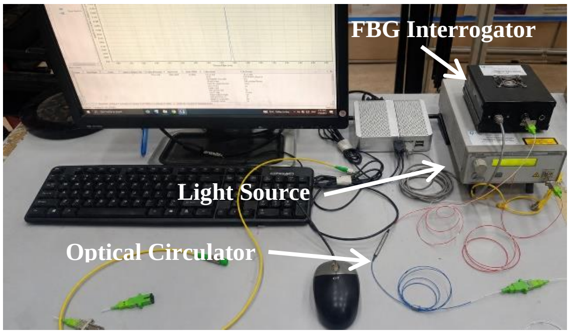

Fig. 3. Actual devices for *FBG* Interrogation system.

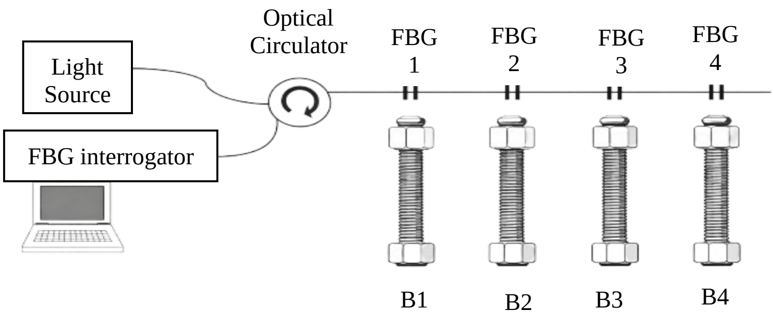

Fig. 4. Schematic illustration of the *FBG* interrogation system.

The experiment focuses on testing a horizontal flange to evaluate the direct behaviour of a single bolt under applied torque. Fig. 5 shows the experimental setup used for this test, which includes the flange, bolts, and the instrumentation required to monitor the strain through *FBG* sensors. The diagram also illustrates the bolt positioning on the flange, where the bolts are arranged symmetrically in a circular pattern. Each bolt ensures uniform load transfer to the selected bolt. This configuration isolates the response of the chosen bolt, allowing for accurate strain measurement. The setup isolated the strain response of a single bolt, ensuring only the selected bolt carried the applied load, preventing load transfer to adjacent bolts. This allows precise measurement of the bolt's strain under varying torque while ensuring data accuracy. Torque was applied according to *ASME-PCC-1-2019* and *ISO-898-1* standards, with three threads engaged on one side of the flange and the remaining threads on the opposite side. Copper-based grease was used for lubrication as recommended in previous studies to reduce friction and achieve consistent tightening (Mascenik & Coranic, 2022). The procedure began by recording the initial wavelength (λ_i) from the *FBG* sensor on bolt 1. Torque was applied in increments of 10 *Nm* using a torque wrench while the wavelength variation was monitored with the Sense software. The software was used to collect and visualize real time wavelength data from the *FBG* sensors, enabling accurate tracking of changes caused by strain and temperature. This process ensured that each loading step was precisely recorded, allowing consistent

https://doi.org/10.24191/jmeche.v23i2.11765

evaluation of the bolt response under applied torque. The initial wavelength (λ_i) represented the unloaded condition, while the final wavelength (λ_f) corresponded to the loaded state, allowing precise determination of strain and stress from the *FBG* response.

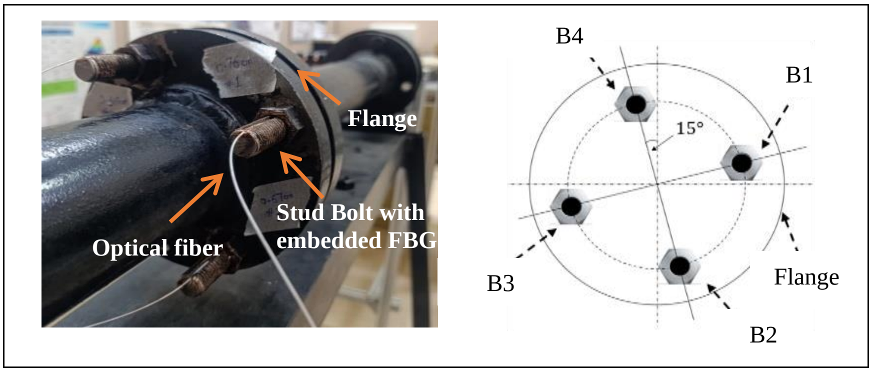

Fig. 5. Positioning of bolts (1 – 4).

After recording the readings, the change in wavelength (λ_f-λ_i) together with the initial Bragg wavelength (λ_i) of the sensor and the effective photoelastic coefficient of 0.22 were put into Equation 2. The effect of temperature was neglected since all experiments were conducted at constant room temperature and the change in temperature) was assumed to be zero as shown in Equation 2. From these values, the axial strain was calculated. Once the strain was obtained, the next step was to determine the stress by applying the Young's modulus of the material.

$$E = \frac{\sigma}{\varepsilon} \tag{4}$$

By using Equation 4, the calculated axial strain (ε) and the Young's modulus (E = 210 *GPa*) are used to calculate the corresponding stress values. The stress and strain for bolt 1 are first determined at an applied torque of 10 *Nm*, and the same procedure is then repeated for bolts 2, 3, and 4 at the same torque level. This process is subsequently carried out for each incremental torque step 10 *Nm*, 20 *Nm*, and continuing up to 80 *Nm*, which represents the maximum torque achievable using the available torque wrench.

RESULTS AND DISCUSSION

Fig. 6 and Fig. 7 show the experimental results of torque against strain and stress, respectively. The results confirm a stable and proportional relationship between the applied torque and the optical strain response, indicating reliable sensor performance throughout the test range. The results also demonstrate a consistent increase in microstrain with applied torque, with slight variations in sensitivity between the bolts, confirming the ability of the *FBG* sensors to provide precise and reliable strain measurements in real time or show a linear relationship between torque and induced stress, further validating the *FBG* sensors' capability for accurate stress monitoring. All bolts displayed a nearly linear increase in microstrain from 10 *Nm* to 80 *Nm*, validating the ability of the *FBG* sensors to measure elastic deformation accurately under stable temperature conditions. The smooth progression of the response curves demonstrates efficient strain transfer between the *FBG* and the bolt, with minimal signal interference, confirming strong mechanical bonding and dependable data accuracy.

https://doi.org/10.24191/jmeche.v23i2.11765

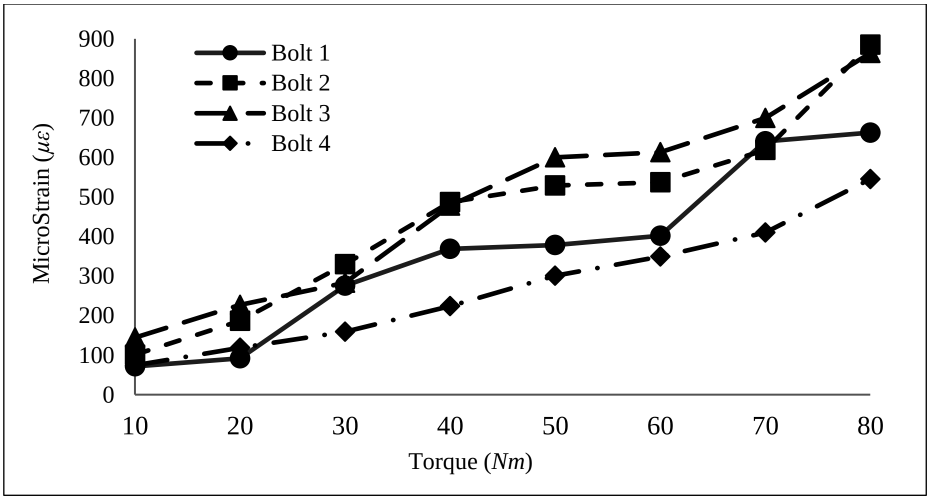

Fig. 6. Strain–torque response for bolts *B1–B4.*

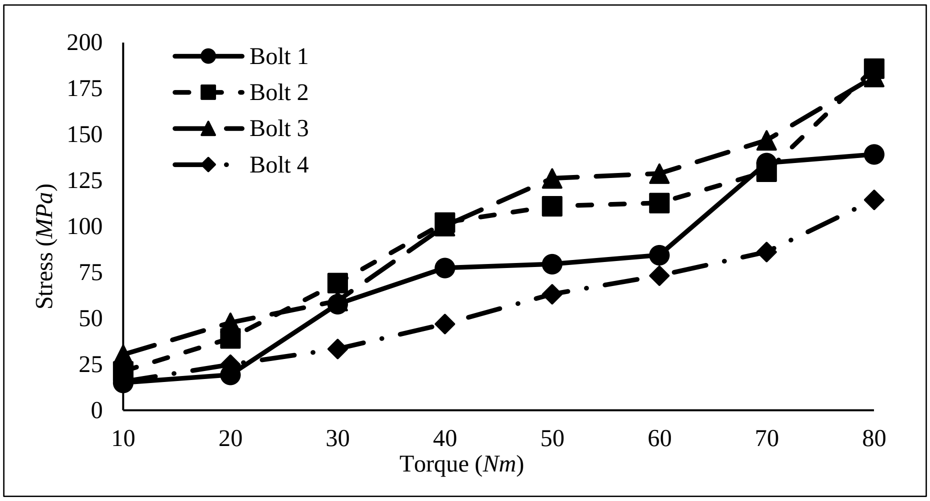

Fig. 6. Stress–torque response for bolts *B1–B4.*

Fig. 8 shows a linear regression was performed on the torque–microstrain data for all four bolts to determine sensitivity, defined as the strain generated per unit torque (*nm/Nm*). Bolt 2 demonstrated the highest sensitivity (0.0123 *nm/Nm*), reflecting its steep torque–strain gradient and indicating pronounced load transfer and localized stress concentration at the shank region. Bolts 1 and 3 exhibited sensitivities of (0.0100 *nm/Nm* and 0.0120 *nm/Nm*), consistent with uniform elastic deformation and stable load-sharing behaviour. Bolt 4 showed the lowest sensitivity (0.0080 *nm/Nm*), suggesting reduced strain responsiveness and more distributed loading. The R^2 values (0.939–0.974) confirm strong linear behaviour across all bolts, validating the reliability of *FBG*-based sensing in capturing torque-dependent strain variations. These results highlight the ability of the embedded *FBG* sensors to resolve bolt-specific mechanical behaviour with high precision, supporting their effectiveness in real-time structural health monitoring of flange assemblies.

https://doi.org/10.24191/jmeche.v23i2.11765

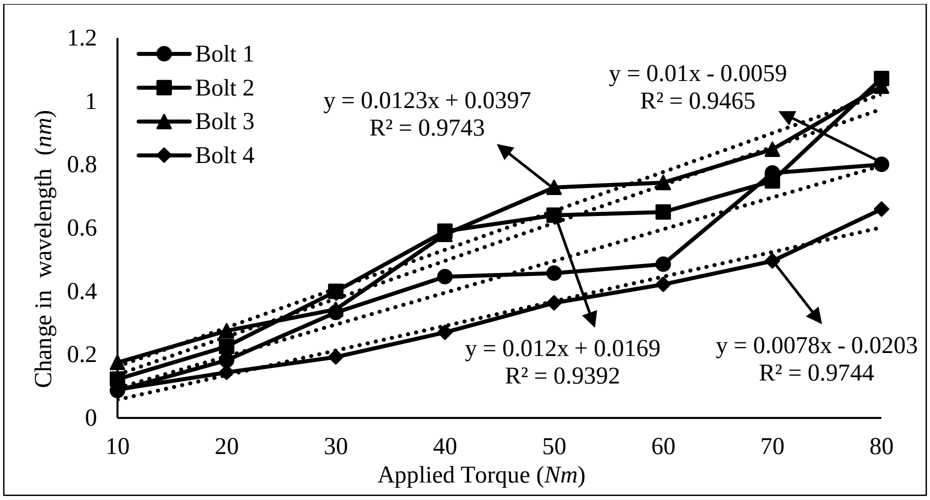

Fig. 7. *FBG* sensitivity response under applied torque.

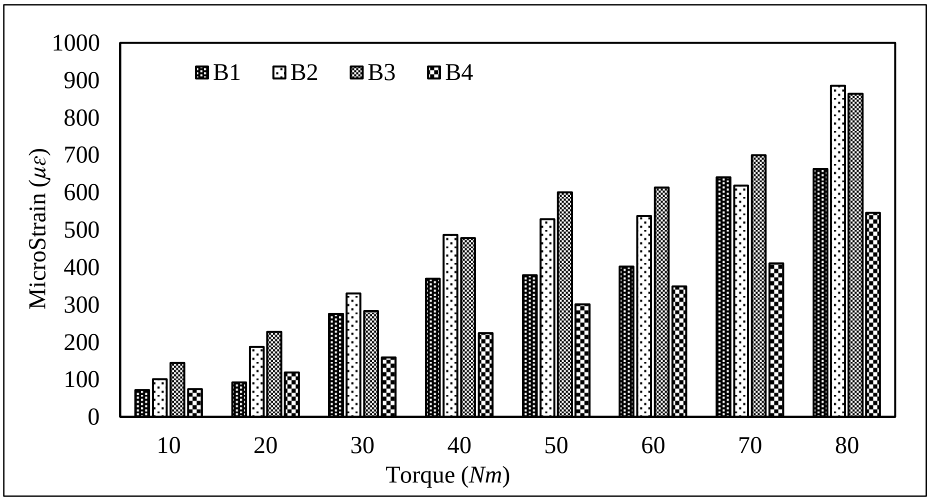

Fig. 9. Bolt-to-bolt comparison of microstrain vs. applied torque for B1–B4.

While Fig. 6 and Fig. 7 establish the relationship between torque, strain, and stress, Fig. 9 and Fig. 10 further resolve this behavior at individual bolt locations. Specifically, Fig. 9 and Fig. 10 present bar chart distributions of strain and stress for bolts *B1* to *B4* under increasing torque. The bar heights increase with torque, confirming a direct dependence on the applied load. Although the overall stress and strain values follow a similar trend for each torque level, bolts *B2* and *B3* generally exhibit higher values than *B1* and *B4*. In particular, *B2* shows the maximum response at 80 *Nm*, indicating a non-uniform load distribution along the bolts. This variation is likely due to thread interaction and contact effects, while the differences in bar height highlight localized stress concentrations and position-dependent responses.

https://doi.org/10.24191/jmeche.v23i2.11765

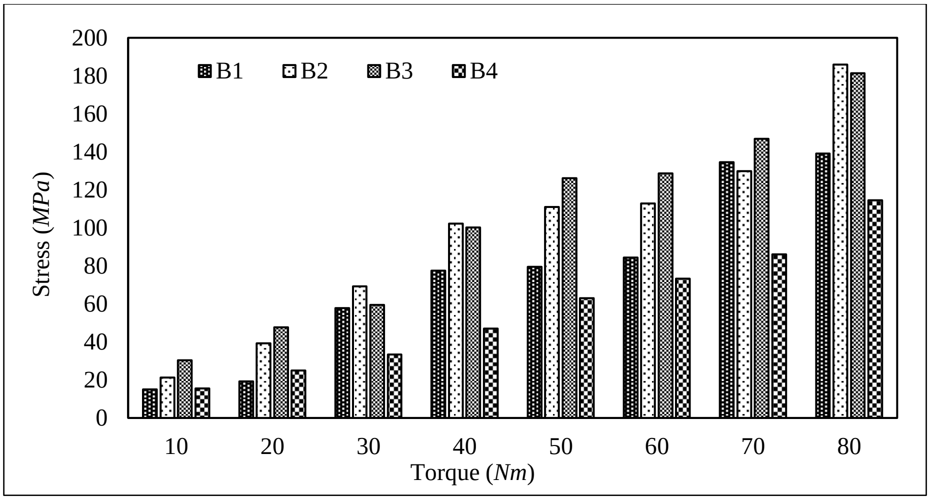

Fig. 10. Bolt-to-bolt comparison of stress vs. applied torque for *B1–B4*.

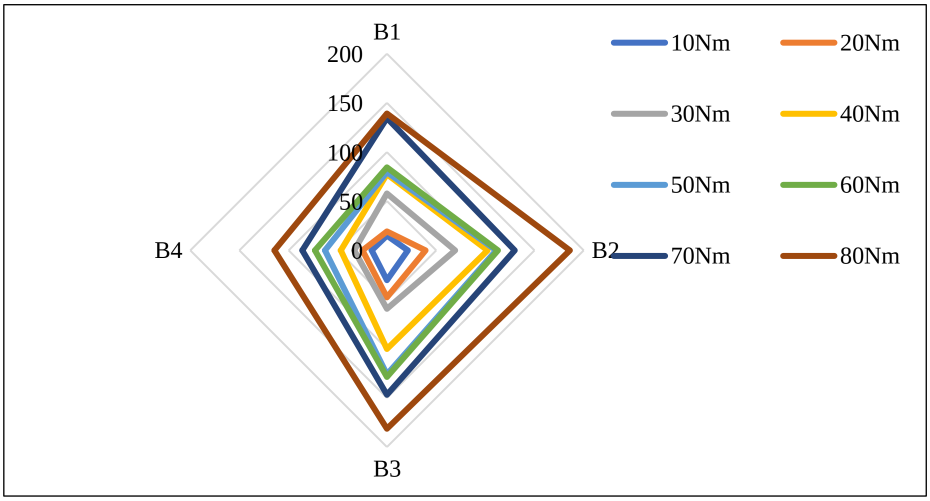

Fig. 11. Radar plot of bolt stress response (*B1–B4*) under varying torque levels.

Fig. 11 presents a radar chart that provides a consolidated representation of the torque dependent stress responses for all bolts. The chart clearly visualizes the stress variations across the bolts, emphasizing Bolt 2's higher stress sensitivity and more effective load transfer under increased torque. Bolt 2 exhibits the steepest increase, indicating higher stress sensitivity and more effective load transfer at higher torque levels, consistent with the stress data observed in Fig. 8. The variations in the slopes of the stress curves across bolts highlight differences in local stress concentration and provide insights into load distribution uniformity within the assembly. The radar chart also supports the observation that the *FBG*-embedded bolts maintain stable and consistent performance under varying torque conditions, with each bolt displaying distinct yet reliable stress characteristics. The sensitivity ranking of Bolt 4 < Bolt 1 < Bolt 3 < Bolt 2 provides valuable information about the load-sharing behaviour of the bolts that Bolt 4 is the least sensitive to torque changes, and Bolt 2 is the most sensitive.

https://doi.org/10.24191/jmeche.v23i2.11765

In the meantime, Fig. 12 and Table 1 demonstrate that the proposed *FBG* bolt exhibits significantly higher sensitivity, ranging from 0.0080 to 0.0123 *nm/Nm*, compared to the reported range of 0.00139 to 0.00296 *nm/Nm* for conventional *FBG* bolts (Yang et al., 2023). The maximum sensitivity of 0.0123 nm/Nm in the present study indicates a substantially enhanced wavelength response per unit torque, exceeding the reference study's peak value by more than four times. This improvement can be primarily attributed to enhanced strain transfer efficiency and optimized sensor placement. Since the *FBG* response is directly proportional to the induced strain, sensors positioned closer to high-stress regions such as the bolt surface, threads, or load-bearing zones experience greater strain, resulting in larger wavelength shifts. In contrast, the reference study employed sensor embedding at controlled depths and more uniform stress regions, which reduced the effective strain experienced by the *FBG* and consequently limited sensitivity. Additionally, differences in bonding quality, host–sensor interaction, and mechanical coupling between the *FBG* and the bolt material may further influence strain transfer. The proposed design likely improves interfacial strain transmission, minimizing losses due to slippage or strain attenuation. Variations in bolt geometry, thread engagement, and local stress concentration effects also contribute to the observed sensitivity enhancement by amplifying localized strain fields.

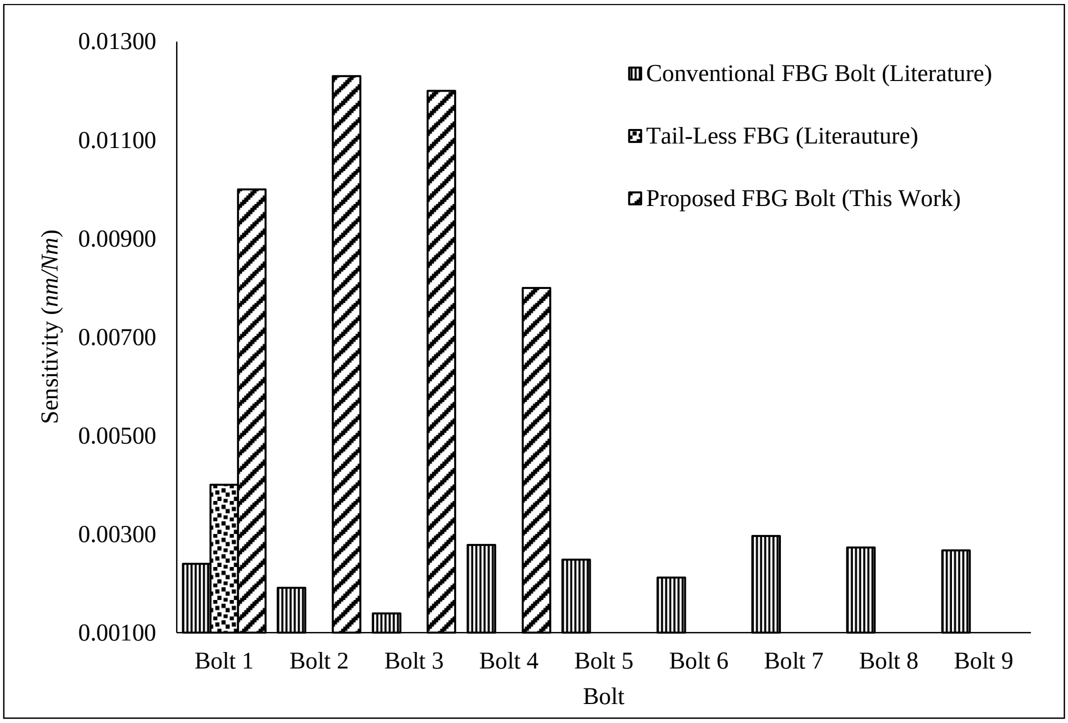

Fig. 12. *FBG* embedded bolt sensitivity comparison.

Table 1. Sensitivity comparison between previous and proposed systems

Study Type	Min (*nm/Nm*)	Max (*nm/Nm*)	Average (*nm/Nm*)
Conventional *FBG* bolt (Literature)	0.00139	0.00296	0.00238
Tail-less (*FBG* bolt) (Literature)	0.00400	0.00400	0.00400
Proposed *FBG* bolt	0.0078	0.01230	0.01058

https://doi.org/10.24191/jmeche.v23i2.11765

Building on the observed enhancement in sensitivity due to improved strain transfer and sensor positioning, the present study also demonstrates strong methodological consistency with the work of Hou et al. (2024) on tailless *FBG* smart bolts. Both approaches employ embedded *FBG* sensing to establish a direct relationship between applied torque and wavelength shift, enabling effective structural health monitoring of bolted systems. Despite this similarity, a key distinction lies in the sensor integration strategy and its influence on both structural integrity and sensing performance. In the present study, the *FBG* sensor is embedded within a shallow longitudinal groove along the shank of M18 grade 8.8 bolts. This configuration preserves the effective load-bearing cross-section, thereby maintaining the original mechanical strength and stiffness of the bolt while still achieving enhanced sensitivity through localized strain concentration. In contrast, Hou et al. introduced a 40 *mm* deep internal cavity within an M24 bolt to accommodate the sensor. Their finite element analysis showed an increase in local strain from approximately $1.470 \times 10^{-3}$to 1.748×10^{-3}under identical loading, indicating a reduction in structural stiffness due to material removal. While the tailless design promotes improved linearity and repeatability by generating a more uniform strain field around the sensor, it compromises structural robustness. Conversely, the groove-based embedding approach in this study leverages naturally occurring stress concentrations at the bolt surface and threads, resulting in higher strain transfer to the *FBG* and, consequently, greater sensitivity. Additionally, this method enhances interfacial bonding, minimizes strain attenuation, and avoids stress discontinuities associated with deep internal modifications.

A further comparative evaluation was conducted between the proposed *FBG*-based sensing system and the full-length *FBG* bolt system reported by Wang et al. (2020). In the referenced study, the wavelength shift–axial load relationship was characterized in terms of applied load (*kN*), providing a consistent baseline for performance assessment. To ensure a direct and meaningful comparison, the same load-based framework was adopted in the present work. As summarized in Table 2 and illustrated in Fig. 13, the proposed sensing system demonstrates a significantly higher sensitivity than the conventional full-length *FBG* bolt. After unit normalization, the proposed system exhibits a sensitivity range of 0.0288–0.0443 *nm/kN*, compared to 0.01067–0.02507 *nm/kN* reported in the previous study, corresponding to an improvement of approximately 2.3 times. This enhancement is also reflected in the average sensitivity, where the proposed system reaches 0.0381 *nm/kN*, substantially exceeding the 0.01670 *nm/kN* of the reference system. The higher slope of the regression line in Fig. 13 (0.0357 for the proposed system versus 0.01429 for Wang et al.) clearly indicates a stronger wavelength response per unit load. From a graphical perspective, Fig. 13 highlights two distinct linear trends. The proposed system exhibits a steeper slope with a lower baseline wavelength (~1548 *nm*), while the reference system shows a more gradual slope at a higher baseline (~1555 *nm*). The steeper slope directly corresponds to higher sensitivity, meaning that for the same incremental load, the proposed sensor produces a larger wavelength shift.

Table 2. Performance comparison of *FBG* sensitivity values

Study Type	Min (*nm/kN*)	Max (*nm/kN*)	Average (*nm/kN*)
Previous Study	0.01067	0.02507	0.01670
Proposed Work	0.0288	0.0433	0.0381

https://doi.org/10.24191/jmeche.v23i2.11765

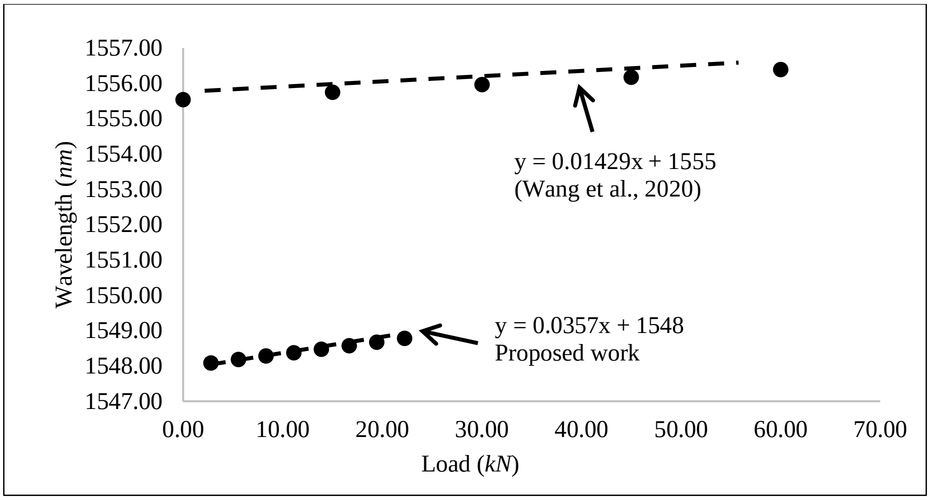

Fig. 13. Selective wavelength comparative response under applied load of proposed work vs Wang et al. (2020).

Overall, the experimental results demonstrate an approximately linear wavelength–load relationship, with R^2 values ranging from 0.939 to 0.974, indicating a stable and repeatable sensor response under applied loading. Although these values are slightly lower than those reported in previous studies, such as Wang et al. (2020), Yang et al. (2023), and Hou et al. (2024), where near-ideal linearity ($R^2 > 0.999$) was achieved but they still remain sufficiently high for reliable engineering applications. The reduced linearity in the present system can be attributed to the more complex loading and sensing conditions. Unlike controlled axial loading environments used in prior studies, the torque-induced loading in bolted joints generates combined stress states, including axial, shear, and contact stresses arising from thread engagement and frictional interaction between mating surfaces. These factors alter the direct proportionality between torque and axial strain, introducing localized strain gradients along the bolt and, consequently, along the embedded *FBG* sensor.

Building on these observations, the enhanced sensitivity of the proposed system further strengthens its practical applicability despite the slight reduction in linearity. The higher wavelength–load response, as previously discussed, reflects improved strain coupling and localized strain amplification within the bolt. This makes the system particularly effective for real-time monitoring of preload and load distribution in bolted connections. In practical industrial environments, where loading conditions are inherently complex, involve frictional losses, and are less controlled than laboratory conditions, the ability to detect small variations in load with higher resolution becomes more critical than achieving near-ideal linearity. Therefore, the proposed approach offers a well-balanced performance by combining adequate linearity with superior sensitivity. This balance enhances its suitability for structural health monitoring applications, enabling early detection of load redistribution, potential loosening, and other integrity-related issues, which are essential for reliable operation and predictive maintenance planning.

CONCLUSION

FBG-embedded stud bolts were shown to enable reliable real-time measurement of bolt strain and preload in bolted flange joints. The sensors exhibited a near-linear torque to microstrain response from 10 to 80 *Nm*, with R^2 values between 0.939 and 0.974, confirming strong linearity and repeatability. Sensitivity varied across bolts, with Bolt 2 showing the highest response (0.0123 *nm/Nm*), followed by Bolt 3 (0.0120 *nm/Nm*), Bolt 1 (0.0100 *nm/Nm*), and Bolt 4 (0.0080 *nm/Nm*), and strain values ranging from approximately

https://doi.org/10.24191/jmeche.v23i2.11765

100 to over 900 $\mu\varepsilon$ at 80 *Nm*. Strain-to-stress conversion using a Young's modulus of 210 *GPa* produced consistent elastic stress levels, validating the measurement approach. These results confirm that *FBG*-embedded bolts can accurately detect preload variation and bolt-level load sharing, even in environments unsuitable for electrical sensors. Although limited to isolated bolts under constant temperature, the study demonstrates the technical feasibility of *FBG*-based monitoring for flange integrity assessment and predictive maintenance in industrial piping systems. Note that the study did not consider elastic interaction, internal pressure, or long-term creep. Future research should focus on advancing and validating *FBG*-embedded bolt technology through full-scale assembly testing for elastic interaction, tightening sequences, internal pressure, and axial loading. The implementation of temperature compensation techniques or dual-parameter *FBG* sensors is needed to distinguish thermal and mechanical effects, while long-term and high-temperature evaluations should assess creep, relaxation, and sensor durability. This research establishes the technical feasibility of using *FBG*-embedded bolts as a practical and sustainable solution for monitoring flange integrity and preventing leakage in industrial piping systems.

ACKNOWLEDGEMENTS

The authors gratefully acknowledge the Research and Innovation Department of Universiti Malaysia Pahang Al-Sultan Abdullah (*UMPSA*) for supporting this work through the internal research grant, RDU233005, at Faculty of Mechanical and Automotive Engineering Technology (*FTKMA*), *UMPSA.*

CONFLICT OF INTEREST STATEMENT

The authors declare that they have no known competing financial interests or personal relationships that could have appeared to influence the work reported in this paper.

AUTHORS' CONTRIBUTIONS

The contributions of the authors reflect a coordinated effort in conducting the research and preparing the manuscript. Muhammad Abdullah carried out the main body of the work including the design of experiments data collection analysis and interpretation of results and preparation of the manuscript. His role ensured that the study was developed in a clear and systematic manner from experimentation to writing. Mohd Hafizi Zohari provided overall supervision and guidance throughout the research process and contributed to improving the structure clarity and technical quality of the manuscript. Ihsan Naiman Ibrahim supported the experimental work and assisted in data collection and validation which helped strengthen the reliability of the results. All authors contributed to reviewing the manuscript and approved the final version for submission.

DECLARATION OF GENERATIVE AI IN THE WRITING PROCESS

The use of generative AI in this work was limited to improving the clarity and readability of the manuscript. During the preparation of this work the authors used ChatGPT to refine sentence structure and enhance the overall flow of the text. This support helped in presenting the ideas in a more organized and understandable manner. After using this tool, the authors carefully reviewed and revised the content to ensure accuracy and

https://doi.org/10.24191/jmeche.v23i2.11765

consistency. The authors take full responsibility for the final content and confirm the integrity of the entire manuscript.

DATA AVAILABILITY/ SUPPLEMENTARY MATERIALS

All data generated or analysed during this study are included in this published article.

ETHICS STATEMENT

This study was conducted in accordance with established safety and ethical standards and did not involve any human or animal subjects. All experimental procedures were carried out following the institutional Safety Health and Environmental protocols of Universiti Malaysia Pahang Al-Sultan Abdullah (UMPSA). The research focused solely on mechanical systems and measurements without any biological or human participation. Therefore, no ethical approval or informed consent was required for this study.

REFERENCES

Abdullah, M., Zohari, M. H., Ramli, R., Shukri, N. A. A. M., & Priyandoko, G. (2025). Investigation of stud bolts with incorporated Fiber Bragg Grating sensors for real-time flange bolt integrity monitoring. Journal of Advanced Research in Applied Mechanics, 141(1), 148–162. https://doi.org/10.37934/aram.141.1.148162

Aycock, J. B., Wilson, J., & Bausman, A. (2019). Variables affecting nut factors in bolted flange connections. Proceedings of the ASME 2019 Pressure Vessels and Piping Conference. Volume 2: Computer Technology and Bolted Joints (pp. 1-10). ASME Publisher. https://doi.org/10.1115/PVP2019-93721

Bhatti, H. S., Aizzuddin, A. M., Hadeed, M., Vorathin, E., & Mohamad, H. (2024). Review of fibre optic geophones and accelerometers for potential application in seismic acquisition for carbon storage monitoring. Optics & Laser Technology, 179, 111368. https://doi.org/10.1016/j.optlastec.2024.111368

Bouzid, A. H., & Nechache, A. (2004). Creep modeling in bolted flange joints. Proceedings of the ASME/JSME 2004 Pressure Vessels and Piping Conference. Analysis of Bolted Joints (pp. 49–56). ASME Publisher. https://doi.org/10.1115/PVP2004-2621

Bouzid, A. H., & Nechache, A. (2010). The modelling of bolted flange joints used with disc springs and tube spacers to reduce relaxation. International Journal of Pressure Vessels and Piping, 87(12), 730–736. https://doi.org/10.1016/j.ijpvp.2010.09.001

Cloostermans, B., Pronk, D., Bruckenburg, B., Goossens, S., Baghdasaryan, T., & Berghmans, F. (2025). Bolted flange connection leakage: a systematic review of monitoring challenges and technologies. IEEE Sensors Reviews, 2, 1-16.

Hadeed, M., Bhatti, H. S., Aizuddin, A. M., Vorathin, E., & Mohamad, H. (2025). Review of fibre optic hydrophones for potential application in offshore carbon storage monitoring. Sensors and Actuators A: Physical, 386, 116341. https://doi.org/10.1016/j.sna.2025.116341

Hou, D., Zheng, M., Yang, Z., Li, R., & Li, X. (2024). A tailless FBG smart bolt with good performance.

https://doi.org/10.24191/jmeche.v23i2.11765

Heliyon, 10(18), e37772. https://doi.org/10.1016/j.heliyon.2024.e37772

Khan, N. B., Abid, M., Jameel, M., & Wajid, H. A. (2017). Joint strength of gasketed bolted pipe flange joint under combined internal pressure plus axial load with different (industrial and ASME) bolt-up strategy. Proceedings of the Institution of Mechanical Engineers, Part E: Journal of Process Mechanical Engineering, 231(3), 555–564. https://doi.org/10.1177/0954408915614460

La Salandra, V., Di Filippo, R., Bursi, O. S., Paolacci, F., & Alessandri, S. (2016). Cyclic response of enhanced bolted flange joints for piping systems. Proceedings of the ASME 2016 Pressure Vessels and Piping Conference. Volume 8: Seismic Engineering (pp. 1-10). ASME Publisher. https://doi.org/10.1115/PVP2016-63244

Mascenik, J., & Coranic, T. (2022). Experimental determination of the coefficient of friction on a screw joint. Applied Sciences, 12(23), 11987. https://doi.org/10.3390/app122311987

Moravcik, M., Kralovanec, J., & Sifta, R. (2026). Monitoring and analysis of existing post-tensioned bridge using FBG sensors. Cogent Engineering, 13(1), 2639837. https://doi.org/10.1080/23311916.2026.2639837

Nechache, A., & Bouzid, A. H. (2008). The effect of cylinder and hub creep on the load relaxation in bolted flanged joints. Journal of Pressure Vessel Technology, 130(3), 031211. https://doi.org/10.1115/1.2937739

Nechache, A., & Bouzid, A. H. (2007). Creep analysis of bolted flange joints. International Journal of Pressure Vessels and Piping, 84(3), 185–194. https://doi.org/10.1016/j.ijpvp.2006.06.004

Nechache, A., Bouzid, A. H., & Lê, V. N. (2004). Analytical modeling of a bolted flange joint subjected to creep relaxation. International Conference on Nuclear Engineering, Volume 1 (pp. 705–712). ASME Publisher. https://doi.org/10.1115/icone12-49243

Nelson, N. R., Prasad, N. S., & Sekhar, A. S. (2023). Structural integrity and sealing behaviour of bolted flange joint: a state of art review. International Journal of Pressure Vessels and Piping, 204, 104975. https://doi.org/10.1016/j.ijpvp.2023.104975

Park, J. S., & Park, K. S. (2014). Implementation of FBG sensor network system for monitoring structure deformation. The Journal of the Korea Institute of Electronic Communication Sciences, 9(8), 841–846. https://doi.org/10.13067/JKIECS.2014.9.8.841

Radzi, M. P., & Zohari, M. H. (2023). A review on the bolted flange looseness detection method. International Conference on Mechanical Engineering Research 2021 (pp. 287–298). Springer. https://doi.org/10.1007/978-981-19-1577-2_22

Silva, R. D., & Sakamoto, J. M. S. (2026). Design, calibration and characterization of a fiber optic triaxial accelerometer based on Fiber Bragg Gratings. Sensors, 26(5), 1588. https://doi.org/10.3390/s26051588

Todd, M. D., Nichols, J. M., Trickey, S. T., Seaver, M., Nichols, C. J., & Virgin, L. N. (2006). Bragg grating-based fibre optic sensors in structural health monitoring. Philosophical Transactions of the Royal Society A: Mathematical, Physical and Engineering Sciences, 365(1851), 317–343. https://doi.org/10.1098/rsta.2006.1937

Wang, P., Zhang, N., Kan, J., Xie, Z., Wei, Q., & Yao, W. (2020). Fiber Bragg grating monitoring of full-bolt axial force of the bolt in the deep strong mining roadway. Sensors, 20(15), 4242. https://doi.org/10.3390/s20154242

Yang, W. S., Chiang, C. C., & Hsu, H. C. (2023). Monitoring torque in bolts using an embedded fiber

https://doi.org/10.24191/jmeche.v23i2.11765

Bragg grating sensor. Optik, 291, 171294. https://doi.org/10.1016/j.ijleo.2023.171294

Zheng, X. T., Cheng, Y., & Yu, J. Y. (2016). The analysis of bolted flange joints under internal pressure at high temperature. Applied Mechanics and Materials, 853, 335–340. https://doi.org/10.4028/www.scientific.net/amm.853.335

Zhu, L., Bouzid, A. H., Hong, J., & Zhang, Z. (2018). Elastic interaction in bolted flange joints: an analytical model to predict and optimize bolt load. Journal of Pressure Vessel Technology, 140(4), 041202. https://doi.org/10.1115/1.404042